

## Miscibility of Polyolefin Blends

J. Luettmmer-Strathmann<sup>†</sup> and J. E. G. Lipson\*

Department of Chemistry, Dartmouth College, Hanover, New Hampshire 03755

Received September 17, 1998; Revised Manuscript Received December 2, 1998

**ABSTRACT:** Phase separation in polymers is important for many technical applications but is difficult to predict theoretically. Recently, extensive experimental studies on the miscibility of polyolefins revealed that these systems display a wider variety of mixing behavior than their chemical similarity suggests. In order to predict phase diagrams of polyolefin blends from pure component properties, we have developed a method in which small scale simulations of local interactions are combined with an analytical model for the thermodynamics, the Born–Green–Yvon lattice model. In this work, we present results for a variety of polyolefin blends and show that the new approach yields qualitatively correct results for phase separation in these blends, including the effects of varying pressure and molar mass of the components on phase separation temperatures.

## 1. Introduction

Prediction of miscibility in polymer blends is a non-trivial task, even when the problem is confined to that of a compressible binary mixture. Hampering these efforts in the past has been the lack of data on a series of mixtures in which systematic changes have been made, either to the structure of the components and/or the nature of the interactions between them. In the last few years such data have begun to appear<sup>1–5</sup> for a series of polyolefin blends and this has stimulated recent theoretical interest<sup>6–12</sup> in the area of blend miscibility. The availability of experimental results in which local polymer structure, temperature, pressure and blend composition are all variables is the motivation for this work, in which we compare experimental data with predictions from the Born–Green–Yvon (BGY) lattice theory for binary compressible blends.

The polymers of interest are all hydrocarbons, and their skeletal structures are shown in Figure 1. Polyethylene (PE) is the simplest, being a straight chain hydrocarbon. Polypropylene has two methyl branches per repeat unit and can be either head-to-tail (denoted PP) or head-to-head (hhPP). The alternating copolymer of PE and PP has one branch per repeat unit (PEP), while polyisobutylene (PIB) is the most heavily branched of the set, with four methyl branches per repeat unit. Choosing pairs from among this group yields a range of behavior. For example, PEP exhibits an upper critical solution temperature (UCST) when blended with PE<sup>1</sup> or hhPP,<sup>2</sup> but a lower critical solution temperature (LCST) when blended with PIB.<sup>2</sup> Even PP and hhPP show differences, the former being more miscible with both PEP<sup>2</sup> and PIB<sup>3</sup> than the latter.

In recent work using the lattice BGY theory, we studied alkane mixtures and solutions of polyethylene with alkanes.<sup>13</sup> Requiring only data on the pure components, we were able to show excellent agreement between experimental results and theoretical predictions for solution vapor pressures, volume changes on mixing and their pressure dependence (alkane mixtures) and LCSTs and coexistence curves (PE–alkane solutions). One issue in turning to polyolefin blends is the

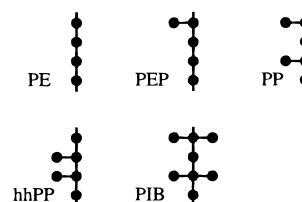


**Figure 1.** United atom representation of the polyolefins considered in this work. Shown are the repeat units with four carbon atoms in the backbone.

extent to which we can push this very simple approach to mixtures. The larger goal is to demonstrate that the lattice BGY theory is capable both of making predictions about such blends and of providing insight into the issues associated with their limited miscibility.

The remainder of the paper is organized as follows: In section 2 we describe the lattice BGY model for compressible fluids and their mixtures, and discuss the microscopic parameters in the theory. All but one of the system-dependent parameters of a mixture are obtained from a comparison with experimental data for the pure components. The remaining parameter characterizes the mixed interaction energy. In section 3 we follow the approach of other theoretical treatments, cf. refs 9 and 14, and use experimental data to determine the value of this parameter. As a result the BGY theory is able to make predictions about the effects of molar mass and pressure on miscibility which are in excellent agreement with experimental results. This is in contrast to results obtained using the well-known geometric mean approximation for the mixed interaction energy. In section 4 we change our approach completely, outlining how small-scale simulations may be used to determine the mixed interaction energy. The resulting theoretical predictions, outlined in section 5, are, for most of the blends, in close agreement with experiment. The cases where the predictions fail provide insight into the physical mechanisms at work and suggest extensions of the simulation procedure to capture these effects. As noted before, these BGY results do not require data on the blends, only on the pure fluids. We discuss our results and draw conclusions in section 6. The determination of the characteristic parameters of the polymeric fluids is summarized in the Appendix.

<sup>†</sup> Present address: Department of Physics, The University of Akron, Akron, OH 44325-4001.

## 2. Born–Green–Yvon Lattice Model for Compressible Fluids

In the BGY lattice model, a molecule of species  $i$  is assumed to occupy  $r_i$  contiguous sites on a lattice having coordination number  $z$  and a volume  $V = vN_0$ , where  $N_0$  is the number of lattice sites and  $v$  is the volume per site. As in earlier work,<sup>15–17</sup> we set  $z = 6$  corresponding to the simple cubic lattice. The site fractions  $\phi_i$ ,  $\phi_h$ , and  $\phi$  are defined as  $\phi_i = r_i N_i / N_0$ ,  $\phi_h = N_h / N_0$ , and  $\phi = 1 - \phi_h$ , where  $N_i$  is the number of molecules of component  $i$  and  $N_h$  is the number of empty sites or holes. Each molecule of species  $i$  has  $q_i z = r_i(z - 2) + 2$  interaction sites, leading to the definition of concentration variables  $\xi_i = q_i N_i / (N_h + \sum_j q_j N_j)$  and  $\xi_h = N_h / (N_h + \sum_j q_j N_j)$  which account for the nearest-neighbor connectivity of the molecules. The interaction energy associated with nonbonded nearest neighbors of the same species is  $\epsilon_{ii}$ , while  $\epsilon_{ij}$  corresponds to interactions between unlike nearest neighbor segments. The Born–Green–Yvon integral equation hierarchy links distribution functions of successively higher order. By closing the hierarchy at the level of pairwise interactions using the Kirkwood superposition approximation and then assuming pair independence for all but the particular pair of interest, Lipson<sup>18</sup> was able to derive simple expressions for the probabilities of the different types of nearest neighbor contacts. Summing the product of these probabilities times the relevant energetic contributions,  $\epsilon_{ii}$  or  $\epsilon_{ij}$ , yielded a closed-form expression for the internal energy of the lattice mixture. Chain connectivity is accounted for through the site fractions,  $\xi$ , and the three parameters,  $r$ ,  $\epsilon$  and  $v$  completely characterize each component. For multicomponent systems there will also be energetic contributions arising from mixed-component interactions, and these are characterized by the  $\epsilon_{ij}$  terms. Since we do not use a literal mapping of the structure of each polymeric repeat unit onto the lattice, as is done in lattice cluster theory, for example,<sup>6–9</sup> the values of these parameters reflect both the chemical and the topological nature of each fluid in the system. It is worth noting that the mapping between  $r$  and  $q$ , and therefore between  $\phi$  and  $\xi$ , does not change as a result of going from linear to branched polymers. In addition, at finite pressures (i.e. all experimentally realizable pressures) the system is compressible, and therefore all of the energetic parameters will contribute. The temperature dependence of the internal energy is used in obtaining an analytic expression for the free energy via a Gibbs–Helmholtz relationship. This requires an approximation for the entropy of the system at infinite temperature, and for this we use Guggenheim's result.<sup>19</sup> Of course, it is only at infinite temperatures that the system is considered to be randomly mixed; at finite temperatures nonrandom contributions to the entropy play a role, and these arise out of the BGY theory itself. This is in contrast to other approaches which do assume random mixing, such as the lattice fluid<sup>20</sup> and Guggenheim<sup>19</sup> theories. In previous work we have shown that at infinite temperature, under certain conditions, these descriptions can be obtained as limiting results of the BGY theory.<sup>15</sup> The BGY result for the dimensionless configurational Helmholtz free energy per lattice site,  $\hat{a}$ , of a  $K$ -component mixture is given by

$$\hat{a} = \sum_{i=h,1}^K \left( \frac{\phi_i}{r_i} \ln \phi_i + \frac{q_i z \phi_i}{2r_i} \left\{ \ln \left[ \frac{\xi_i}{\phi_i} \right] - \ln [\xi_h + \sum_{j=1}^K \xi_j \exp(-\beta \epsilon_{ij})] \right\} \right) \quad (1)$$

where  $\beta = 1/(k_B T)$ ,  $T$  is the temperature and  $k_B$  is Boltzmann's constant. Accordingly, the Helmholtz free-energy density  $A/VT$  is given by

$$A/VT = k_B \hat{a} / v + a_0 \quad (2)$$

where  $a_0$  is a caloric background not needed in this work. All thermodynamic properties of a mixture can now be derived from the thermodynamic relation

$$d(A/VT) = (U/V) d(1/T) + \sum_{j=1}^K (\mu_j/T) d(\rho_j) \quad (3)$$

where  $U$  is the internal energy of the system, and where  $\rho_j = N_j/V = \phi_j/r_j v$  and  $\mu_j$  are the number density and chemical potential of component  $j$ , respectively. The pressure  $P$  and the chemical potentials  $\mu_i$ , for example, are given by

$$P = -\frac{1}{\beta v} \left[ \hat{a} - \sum_{j=1}^K \phi_j \left( \frac{\partial \hat{a}}{\partial \phi_j} \right)_{\beta, \phi_{k \neq j}} \right], \quad \mu_i = \frac{r_i}{\beta} \left( \frac{\partial \hat{a}}{\partial \phi_i} \right)_{\beta, \phi_{k \neq i}} \quad (4)$$

Phase transitions in binary blends are conveniently discussed in terms of the total molar density  $\rho = \rho_1 + \rho_2$  and the mole fraction  $x = \rho_2/\rho$ . The thermodynamic field conjugate to the mole fraction  $x$  is the difference of the chemical potentials  $\mu = \mu_2 - \mu_1$ . In terms of these variables, the conditions for a point  $T_c$ ,  $P_c$ ,  $x_c$  on the critical line of a binary mixture take the form<sup>21</sup>

$$\left( \frac{\partial \mu}{\partial x} \right)_{T,P} = 0, \quad \left( \frac{\partial^2 \mu}{\partial x^2} \right)_{T,P} = 0 \quad (5)$$

The first of the two equations defines the spinodal while the second one implies that, for a given pressure, the critical point is an extremum of the spinodal in the  $T$ - $x$  plane. Hence, lower and upper critical solution temperatures (LCST's and UCST's) correspond to the minimum and maximum of their spinodals, respectively. For temperatures  $T < UCST$  or  $T > LCST$ , the mixture can separate into two phases of different mole fractions  $x_I$  and  $x_{II}$ . For a given pressure  $P$ , the coexisting phases satisfy

$$\mu(T, P, x_I) = \mu(T, P, x_{II}), \quad \mu_1(T, P, x_I) = \mu_1(T, P, x_{II}) \quad (6)$$

The mass fraction  $c$  of component 2 is given by

$$c = M_2 x / (M_2 x + M_1 (1 - x)) \quad (7)$$

where  $M_1$  and  $M_2$  are the molar masses of component 1 and 2, respectively. Compositions of polymer blends are typically quoted in terms of nominal volume fractions. For the polyolefins considered here, the volume fraction is numerically very close to the mass fraction  $c$  defined in eq 7 which will be used throughout this paper.

When the BGY lattice model is applied to binary mixtures, eqs 1–4 are evaluated with  $K = 2$ . The total molar density  $\rho = \rho_1 + \rho_2$  and the mole fraction  $x = \rho_2/\rho$

**Table 1. Miscibility Results for the Polyolefin Blends Considered in this Work<sup>a</sup>**

components; molar masses	experimental data	ref	$g = 1$ prediction	$(g_{\text{exp}} - 1)/10^{-4}$	$(g_{\text{sim}} - 1)/10^{-4}$	$g_{\text{sim}}$ prediction
PEP/PE; 29 450/23 560	UCST; $T_{\text{tr}}(0.5) = 421 \pm 1$ K	1	compl misc	-4.40	-3.51	UCST; $T_{\text{tr}}(0.5) = 352.6$ K
PEP/hhPP; 59 850/171 780	UCST; $T_{\text{tr}}(0.5) = 340 \pm 16$ K	2	compl misc	-0.75	-2.81	UCST; $T_{\text{tr}}(0.5) = 773.0$ K
PEP/PIB; 59 900/38 600	LCST; $T_{\text{tr}}(0.8) = 318 \pm 5$ K	3	LCST; $T_{\text{tr}}(0.8) = 131.9$ K	8.84	9.09	LCST; $T_{\text{tr}}(0.8) = 326.0$ K
hhPP/PIB; 73 077/137 000	LCST; $T_{\text{tr}}(0.4) = 421 \pm 2$ K	22	LCST; $T_{\text{tr}}(0.4) = 126.7$ K	10.3	2.24	LCST; $T_{\text{tr}}(0.4) = 165.6$ K
PEP/PP; 59850/10920	misc for $c = 0.7$ , 300–400 K	2	compl misc	> -3.1	-0.917	UCST type; compl misc
58000/58700	immisc for $c = 0.5$ , $T \approx 300$ K	23	compl misc	< -0.9		$T_{\text{tr}}(0.5) = 307.7$ K
PP/hhPP; 10 920/26 880	misc for $c = 0.5$ , 300–400 K	2	compl misc	> -4.78	-3.72	UCST; $T_{\text{tr}}(0.5) = 239.3$ K
PP/PIB; 59 200/81 600	immisc for $c = 0.5$ , 298–373 K	3	LCST; $T_{\text{tr}}(0.5) = 130.9$ K	< 5.2	17.2	LCST; $T_{\text{tr}}(0.5) = 659.9$ K
PP/PE; 100 000/100 000	immisc for $c = 0.5$ , $T \approx 470$ K	4	immisc for $c = 0.5$ , $T \approx 470$ K	< 0.5	-3.96	immisc for $c = 0.5$ , $T \approx 470$ K
hhPP/PE; 100 000/100 000	immisc for $c = 0.5$ , $T \approx 470$ K	4	misc for $c = 0.5$ , $T \approx 470$ K	< -0.2	-3.30	immisc for $c = 0.5$ , $T \approx 470$ K
PIB/PE; 100 000/100 000	immisc for $c = 0.5$ , $T \approx 470$ K	4	immisc for $c = 0.5$ , $T \approx 470$ K	< 20.0	0.35	immisc for $c = 0.5$ , $T \approx 470$ K

<sup>a</sup>  $T_{\text{tr}}(c)$  indicates the phase transition temperature at the mass fraction  $c$  of component 2; all results are for  $P = 0.1$  MPa.

of the mixture are related to the site fractions  $\phi_1$  and  $\phi_2$  by

$$\rho = \frac{1}{v} \left( \frac{\phi_1}{r_1} + \frac{\phi_2}{r_2} \right), \quad \frac{1}{x} = 1 + \frac{\phi_1}{r_1} \frac{r_2}{\phi_2} \quad (8)$$

In addition to the system-dependent parameters  $r_1$ ,  $r_2$ ,  $v$ ,  $\epsilon_{11} \equiv \epsilon_1$ , and  $\epsilon_{22} \equiv \epsilon_2$  which are determined from a comparison with experimental  $PVT$  data as described in the Appendix, a value is required for the strength of the mixed interaction  $\epsilon_{12}$ . In earlier work on phase coexistence in mixtures of unbranched chain molecules,<sup>13,17</sup> Berthelot's geometric-mean combining rule

$$\epsilon_{\text{geo}} = -\sqrt{\epsilon_{11}\epsilon_{22}} \quad (9)$$

yielded good results. In this work, we represent the mixed interaction  $\epsilon_{12}$  as

$$\epsilon_{12} = g\epsilon_{\text{geo}} \quad (10)$$

where the correction factor  $g$  is introduced to capture the effect of different small scale architectures on the mixed interactions. We should point out that the  $g$  factor introduced here does not describe a scaling property of the interaction potential, but defines an *effective* mixed interaction parameter which reflects the different arrangements of the side groups of the polymers. The following two sections focus on the determination of the geometric correction  $g$ . From a comparison with experimental phase-transition data we show first in section 3 that a small correction is indeed sufficient to reproduce the miscibility of the polyolefin blends considered here. The simulation method presented in section 4 is our first attempt at predicting the values of the correction and thus phase diagrams of the blends from pure component properties alone. The comparison with experimental data in section 5 shows that the simulation values  $g_{\text{sim}}$  for the corrections yield excellent results for some of the blends but that effects beyond the packing of straight chain segments play an important role in the miscibility of other blends.

### 3. Determination of the Correction Factor from a Comparison with Experimental Data

Miscibility of polyolefin blends has been studied experimentally by a variety of techniques, most notably neutron and light scattering.<sup>1–5,22</sup> For some polyolefin blends, temperatures for the phase transition between miscibility and immiscibility have been established from cloud point determinations; for other blends, only qualitative observations have been made. In cases

**Table 2. System-Dependent Parameters for the Polyolefins Considered in This Work ( $M_0 = 170\,000$ ,  $v_0 = 0.013$  L/mol)**

polyolefin	$\epsilon$ (J/mol)	$r$	$v$ (L/mol)	$(rv)/(v_0M_0)$
hdPE	-1977.5	21068.4	0.00876846	0.0835916
PEP	-2000.0	19025.8	0.00972039	0.0836824
aPP	-2040.7	16511.7	0.0113939	0.0851279
hhPP	-2027.8	18575.1	0.00972421	0.0817322
PIB	-2208.1	18547.3	0.0094158	0.0790216

where values for phase transition temperatures at a given composition are available, we are able to determine a value  $g_{\text{exp}}$  for the correction factor in eq 10; if only qualitative information is available, we employ it to determine bounds on the correction factor. The experimental data used for this purpose are summarized in the first two columns of Table 1. For some blends, more than one experimental data point is available, for example at different molar masses of the components or at different compositions. In that case, we use one point to determine a value for  $g_{\text{exp}}$  and use the remaining information to test our predictions based on  $g_{\text{exp}}$ .

For each blend of interest, we start by employing the BGY lattice model, cf. eqs 1–4, with the system-dependent parameters of Table 2 and eq 15 and the mixed interaction in the geometric mean approximation, i.e.  $g = 1$  in eq 10. By numerically solving eqs 5 at the given pressure, here 0.1 MPa, the predicted critical points of the blend, if any, are located and the coexistence curve is calculated from eq 6. In the third column of Table 1, we present the miscibility predictions from the BGY lattice model in conjunction with Berthelot's geometric mean combining rule,  $g = 1$ . A comparison with the corresponding experimental data shows that the geometric mean approximation predicts qualitatively correct LCST phase diagrams for the PIB blends, but the phase transition temperatures are too small; i.e. the predicted miscibility is too small. On the other hand, for blends exhibiting UCST phase diagrams like PEP/PE and PEP/hhPP the geometric mean approximation predicts no phase separation; i.e., the predicted miscibility is too large and there is no qualitative agreement between predicted and observed phase diagrams.

As it turns out, only small corrections to Berthelot's rule are needed to reproduce the experimental phase separation data: if the value of  $g$  in eq 10 is increased slightly, the calculated miscibility increases while it decreases with decreasing  $g$ . Accordingly, we adjust the value of  $g$  and repeat the calculation of the phase boundaries until experimental and calculated phase transition temperatures for the blend agree. The fourth column in Table 1 contains the values  $g_{\text{exp}}$  determined in this way. The extreme sensitivity of phase behavior to small deviations from the geometric mean has

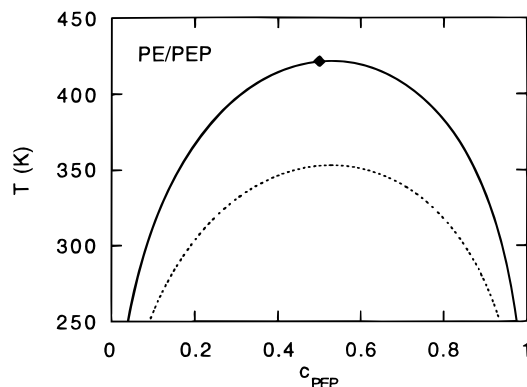


**Figure 2.** Phase coexistence for the PEP/PE blend of Table 2. The diamond indicates the experimental point<sup>1</sup> employed to determine  $g_{\text{exp}}$  on which the first BGY result, solid line, is based. The dotted line is the BGY result based on the simulation value  $g_{\text{sim}}$ . In contrast, the geometric mean approximation for  $\epsilon_{12}$  yields a BGY prediction of complete miscibility.

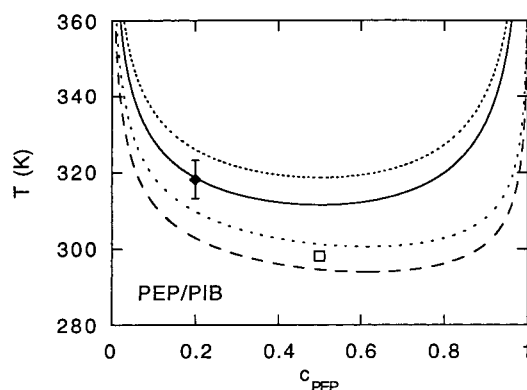


**Figure 3.** Phase coexistence for two PIB/PEP blends with molar masses of 38 600/59 900 (upper curves and diamond) and 81 600/59 900 (lower curves and square), respectively. The diamond indicates the experimental point<sup>4</sup> employed to determine  $g_{\text{exp}}$  on which the first BGY results, solid and dashed lines, are based. The open square indicates temperature and concentration where the second blend was found to be phase-separated. The dotted lines are the corresponding BGY results based on the simulation value  $g_{\text{sim}}$ .

recently been discussed by Dudowicz and Freed<sup>6</sup> and by Graessley, Lohse, and co-workers.<sup>4,14</sup>

In Figure 2 we present the calculated coexistence curve for a PEP/PE blend exhibiting a UCST, where the indicated data point<sup>1</sup> has been used to establish the value for  $g_{\text{exp}}$ . The geometric mean approximation,  $g = 1$ , yielded a prediction of complete miscibility in this case. Also included in the figure is the prediction for the coexistence curve based on our simulation procedure, which will be discussed in detail below. Coexistence curves for two PIB/PEP blends exhibiting LCST phase diagrams are presented in Figure 3. The upper of the two curves contains the experimental data point<sup>4</sup> used to establish the value of  $g_{\text{exp}}$  for PIB/PEP blends. The lower curve is a prediction based on this value of  $g$  for a blend with a different molar mass of PIB. It reproduces the experimental observation<sup>4</sup> that this blend is phase separated at the temperature and concentration indicated by the open square. Blends of hhPP with PIB have recently been investigated by neutron as well as light scattering.<sup>4,5,22</sup> For these blends, we determined the value of  $g_{\text{exp}}$  from a comparison with an experimental value for the LCST obtained by light scattering.<sup>22</sup> Coexistence (binodal) and spinodal curves

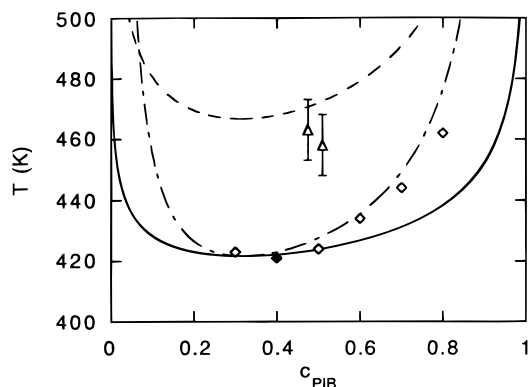


**Figure 4.** Phase diagrams of two hhPP/PIB blends with molar masses of 73 077/137 000 (lower curves) and 27 500/81 600 (upper curve), respectively. The diamond indicates the experimental point<sup>22</sup> employed to determine  $g_{\text{exp}}$  on which the BGY results are based. The solid and dash-dotted lines represent the calculated binodal and spinodal of the first blend, respectively, and the open diamonds indicate experimental<sup>22</sup> spinodal temperatures for this blend. The dashed line represents the calculated coexistence curve of the second blend, and the open triangles indicate experimental phase transition temperatures.<sup>3</sup>

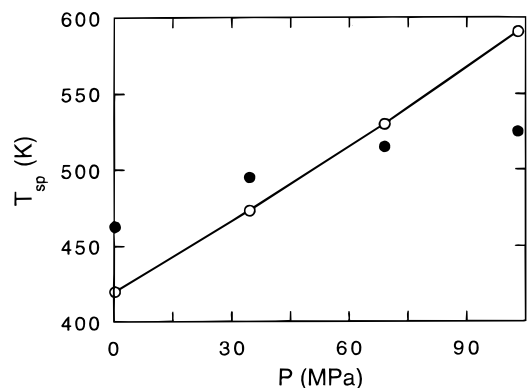


**Figure 5.** Pressure dependence of the spinodal temperature in  $c = 0.5$  hhPP/PIB blend with molar masses 76 400/107 000. The solid line with open circles is the BGY results based on  $g_{\text{exp}}$  determined from the blend in Figure 4, and the full symbols indicate experimental data points.<sup>22</sup>

for this blend along with experimental spinodal temperatures<sup>22</sup> are presented in Figure 4. As can be seen from this graph, critical concentration as well as the shape of the curve are reproduced very well by the BGY lattice model. Also included in the figure are coexistence data for a hhPP/PIB blend of different molar mass; the BGY prediction based on  $g_{\text{exp}}$  agrees well with the experimental points.<sup>3</sup> In our calculations for  $P = 0.1$  MPa, the value  $v_0 = 0.013$  L/mol was chosen to improve the representation of the  $PVT$  surface at low pressures, cf. Figure 11 and the discussion in the Appendix. Very recently, the influence of pressure on the miscibility of hhPP/PIB blends was investigated by neutron scattering. Rabeony *et al.*<sup>22</sup> determined spinodal temperatures at four different pressures for a blend of deuterated PIB ( $M = 107\,000$ ) and hydrogenated hhPP ( $M = 76\,400$ ). In order to describe polymer blends at elevated pressures, we employ the average  $\bar{v} = (v_1 + v_2)/2$  of the volumes quoted in Table 2 for the individual components, instead. The effect of this change of parameters on the calculated value of the LCST is about 10 K, which is small compared to 430 K for the LCST. In Figure 5 we present a comparison between experimental and

calculated spinodal temperatures as a function of pressure.

#### 4. Small Scale Simulations to Predict the Correction Factor Factor

Our emphasis now shifts to predicting values for the correction factor  $g$  through small scale simulations. In order to capture the effect of local architecture on the mixed interaction strength we evaluate interactions between two polyolefin molecules in united atom representation, cf. Figure 1, on a cubic lattice. In this work, we restrict ourselves to sections with straight backbones and to packing effects; i.e. we ignore bending and differences in interaction energies for different sites on the same molecule.

For each of two molecules, consider a straight section composed of three repeat units with given (generally not identical) side group arrangements. The repeat unit in the middle is the section of interest in each case, while the attached units represent the rest of the (long) chains. As depicted in Figure 1, we employ repeat units with four carbon atoms in the backbone for all the polyolefins considered here.

The section of interest of the first molecule is fixed to the origin of a simple cubic lattice and aligned with the  $z$ -axis. The total number  $n_t$  and the coordinates of the nonbonded nearest neighbors (nn) sites are determined as is the maximum number  $c_m = 4s_f$  of possible contacts, where  $s_f$  denotes the number of lattice sites occupied by the fixed section of interest. The section of interest of a PE chain, for example, has  $n_t = 16$  nearest neighbor sites and a maximum of  $c_m = 16$  contacts, while for PIB the values are  $n_t = 24$  and  $c_m = 32$ . Furthermore, the number  $c_s$  of self interactions of the fixed section of interest needs to be counted. For the architectures considered here, this is an issue only with hhPP for which  $c_s = 2$  when its two side groups are on adjacent lattice sites as shown in Figure 1. In all other cases  $c_s = 0$ .

The second molecule is mobile: it is rotated and translated so that its section of interest makes contact with the section of interest of the fixed molecule without overlap between the molecules. The number  $o_k$  of nn sites of the fixed section of interest occupied by the mobile chain are counted as are the number of established contacts  $c_k$  between the two chains. The last two steps are repeated until all possible combined configurations of the two chains are exhausted; then the whole procedure is repeated with different arrangements of the side groups of the molecules. For the results presented here, all side group configurations of the sections of interest and their attachments were considered (exact enumeration procedure). To avoid excessive computation times for systems with a larger number of configurations of the individual molecules, due to longer side chains or bent backbones, for example, a Monte Carlo method can be used to generate representative samples of the individual polymer configurations. The results of the simulation are statistics on the number  $m_k$  of combined configurations corresponding to a given set  $(o_k, c_k, c_s)$  of occupied nn sites and established contacts.

To determine the energy of a combined configuration, we assume that the remaining  $n_t - o_k$  nn sites are filled randomly to a density of  $\xi$ . Here  $\xi = 2\phi/(3 - \phi)$  is the contact density for infinitely long chains corresponding to a total filling fraction of  $\phi$ . (Assuming infinite chains

here has negligible effect on the simulation results since the main density dependence is divided out when the interaction energy per contact is determined, cf. eq 13, but it has the advantage of making the simulation results independent of molar mass.) Accordingly, the energy  $E_k$  for a set of combined configurations  $(o_k, c_k, c_s)$  is given by

$$E_k = \epsilon_{\text{geo}} \left( c_k + \frac{(n_t \xi - o_k)(c_m - c_k - c_s)}{n_t - o_k} + c_s \right) \quad (11)$$

The contributions to the energy  $E_k$  in eq 11 are (from left to right) due to contacts between the fixed and mobile segments, between the fixed segment and its randomly filled nearest neighbor sites, and between two sites on the fixed segment (self-interactions), respectively. The self-interaction contribution to  $E_k$  could be considered more precisely by using  $\epsilon_{11}c_s$  rather than  $\epsilon_{\text{geo}}c_s$  in eq 11. As this contribution is important only in the weighting of the configurations, but is subtracted again when the mixed interaction energy is calculated, see eq 13 below, this has a negligible effect on our results. For a consistent evaluation of results for the different repeat units, with their different numbers  $n_t$  of nn sites, we employ the same number  $n_t = 24$  for each polyolefin in eq 11 and rescale the maximum number of contacts and the number of self interactions according to  $c_m \rightarrow 24 c_m/n_t$  and  $c_s \rightarrow 24 c_s/n_t$ , respectively.

The probability  $P_k$  of a given energy  $E_k$  and the average energy  $\bar{E}$  depend on the temperature  $T$  through

$$P_k = m_k e^{-\beta E_k} / \sum_{k, c_s} m_k e^{-\beta E_k}, \quad \bar{E}(c_s) = \sum_k E_k P_k \quad (12)$$

where  $m_k$  is the multiplicity of the combination  $(o_k, c_k)$ ,  $\beta = 1/RT$ ,  $R$  is the universal gas constant, and  $E_k$  is measured in J/mol. In this way, the simulation with polymer 1 fixed and polymer 2 mobile yields a value for the interaction energy per contact:

$$\bar{\epsilon}_{12} = \sum_{c_s} \frac{\bar{E}(c_s) - c_s \epsilon_{\text{geo}}}{\xi(c_m - c_s)} \quad (13)$$

If the roles of the fixed and the mobile chains are changed and the procedure is repeated, a second value  $\bar{\epsilon}_{21}$  is obtained. The average  $(\bar{\epsilon}_{12} + \bar{\epsilon}_{21})/2$  represents a value for the mixed interaction strength at a given temperature and filling fraction. Since it includes effects of the local architecture we employ this simulation result to obtain estimates for the geometric factor  $g$  in eq 10:

$$(\bar{\epsilon}_{12} + \bar{\epsilon}_{21})/2 \equiv g \epsilon_{\text{geo}} \quad (14)$$

It is worth noting that in general  $\bar{\epsilon}_{12} \neq \bar{\epsilon}_{21}$ . This asymmetry is the result of focusing on the nn sites and the possible contacts of the fixed molecule, while using the mobile section to probe which of those nn sites can be occupied without overlap. It is not difficult to devise an equivalent procedure in which the nn sites of both molecules are considered simultaneously so that a single value for the mixed interaction energy is obtained right away. We have not followed that route here, since we wanted to perform our first simulations using exact enumeration, and the bookkeeping is simplified when the molecules are considered fixed, and then mobile, in turn.

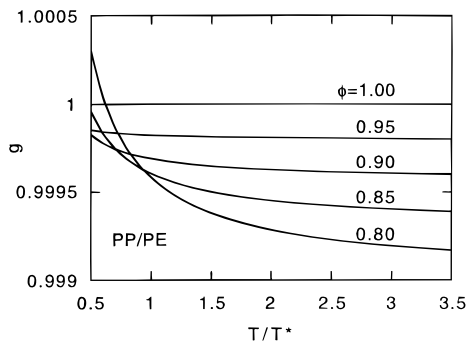


**Figure 6.** Geometric correction  $g$  as a function of reduced temperature for PP/PE blends of different filling fractions.

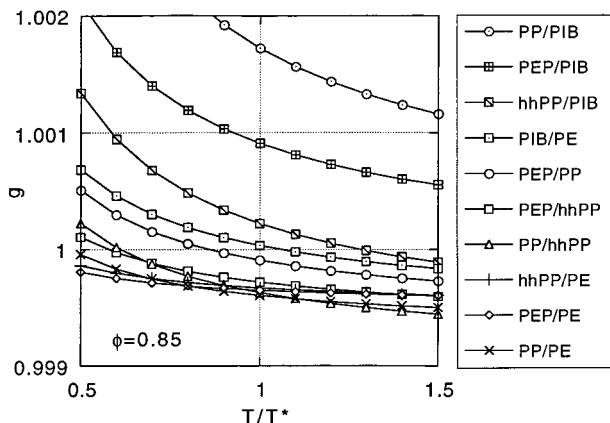


**Figure 7.** Geometric correction  $g$  as a function of reduced temperature for the blends considered in this work at a filling fraction of  $\phi = 0.85$ .

For straight, unbranched chains all nn sites yield a single contact when occupied: setting  $c_k = o_k$  for each  $k$  and  $c_m = n_t$  in eq 11 yields  $E_k = \epsilon_{\text{geo}} c_m \xi$  for all  $k$  so that eqs 12–14 imply  $g = 1$ . Hence, there is no geometric correction for the mixed interactions between two straight, unbranched chain molecules. Chains with side groups, on the other hand, have “special” nn sites whose occupation establishes more than one contact per site. Mixed interactions are (dis) favored compared to the geometric-mean approximation, i.e.  $g > 1$  ( $g < 1$ ), if the molecules can(not) take advantage of each others special sites in many combined configurations. At very low temperature, the energetically favorable combined configurations outweigh the unfavorable ones in eq 12, so that  $g$  increases with decreasing temperature. Finally, independent of chain architectures,  $g = 1$  for  $\phi = 1$  since all nn sites are occupied and all possible contacts are saturated when the lattice is completely filled. These points are illustrated in Figure 6, where we present simulation values for  $g$  as a function of reduced temperature  $T/T^*$ , where  $T^* = \epsilon_{\text{geo}}/R$ , for a variety of filling fractions for interactions between PP and PE molecules. Figure 7 contains the simulation results for  $g$  as a function of reduced temperature and for a filling fraction of  $\phi = 0.85$  for all blends considered in this work.

In the application of the BGY lattice model to polyolefin blends a single value for the mixed interaction strength, cf. eq 10 is employed and requires the extraction of a single value  $g_{\text{sim}}$  for the geometric correction from the simulation results. We choose for  $g_{\text{sim}}$  the value of  $g$  at the characteristic temperature of the blend, i.e.  $T/T^* = 1$ , and a filling fraction  $\phi = 0.85$ , where the choice of  $\phi$  is motivated by the typical hole concentra-

tions encountered in the *PVT* data of the pure components. Values of  $g_{\text{sim}}$  are included in Table 1.

## 5. Phase Transition Results Based on Simulation Values for the Correction Factor

To calculate the phase-diagram predictions based on the simulation values  $g_{\text{sim}}$  for the correction factor, we proceed as we did in section 3: For each of the blends of interest, we numerically solve eqs 5 and 6 with the aid of the BGY lattice model, cf. eqs 1–4, using the system-dependent parameters of Table 2 and eq 15. However, here we use the values of  $g_{\text{sim}}$  in Table 1 along with eq 10 in order to predict the mixed interaction energy. The resulting miscibility predictions from the BGY lattice model in conjunction with the simulation results  $g_{\text{sim}}$  for the correction factor are presented in the last column of Table 1.

A comparison of the simulation predictions with the experimental results and the predictions based on the geometric mean approximation ( $g = 1$ ) in Table 1 yields the following general observations: First of all, the predictions for all phase diagrams, UCST as well as LCST, are qualitatively correct when the simulation value  $g_{\text{sim}}$  is employed in eq 10. This is in contrast to the  $g = 1$  results, where UCST blends are predicted to be completely miscible. Secondly, in all cases where experiment-based values,  $g_{\text{exp}}$ , for the correction factor are available, the signs of  $g_{\text{exp}} - 1$  and  $g_{\text{sim}} - 1$  agree. That means that the simulation results for the mixed interactions predict more miscibility where the geometric mean approximation yields too little and vice versa.

Let us now examine the blends in more detail and start with the PE blends. The PEP/PE blend of Table 1 is experimentally<sup>1</sup> found to have a UCST of about 421 K. The geometric mean approximation yields a prediction of complete miscibility, while a correction factor of  $g_{\text{expt}} - 1 = -4.4 \times 10^{-4}$  in eq 10 allows the BGY lattice model to reproduce the experimental result. The simulation result for the correction factor is  $g_{\text{sim}} - 1 = -3.51 \times 10^{-4}$  yielding a UCST of about 353 K. Coexistence curves based on  $g_{\text{exp}}$  and  $g_{\text{sim}}$  are presented in Figure 2 and show that the simulation prediction, while not quantitative, is quite respectable. For the other PE blends, only qualitative information based on an approximate criterion for miscibility<sup>4</sup> is available. The geometric mean approximation reproduces the expected immiscibility for two of the three blends, while the simulation results correctly predict immiscibility for all three blends.

The PIB blends in Table 1 exhibit LCST phase diagrams. At a mass fraction of 80% PIB, the experimental phase transition temperature of the PEP/PIB blend is found to be about 318 K, while the geometric mean approximation predicts a phase transition temperature of about 132 K. The simulated value  $g_{\text{sim}}$  of the correction factor is very close to the value of  $g_{\text{exp}}$  which allows the BGY lattice model to reproduce the experimental point; i.e.  $g_{\text{sim}} - 1 = 9.09 \times 10^{-4}$  vs  $g_{\text{exp}} - 1 = 8.84 \times 10^{-4}$ . Consequently, the predictions based on  $g_{\text{sim}}$  are excellent and barely outside the experimental error. Coexistence curves based on  $g_{\text{exp}}$  and  $g_{\text{sim}}$  for two PEP/PIB blends are presented in Figure 3. For the hhPP/PIB blend of Table 1, experiments<sup>22</sup> show an LCST at about 421 K leading to a value of  $g_{\text{exp}} - 1 = 10.3 \times 10^{-4}$ . The simulations for this blend yield a value of  $g_{\text{sim}} - 1 = 2.24 \times 10^{-4}$  and an LCST of about 166 K, which is only a small improvement over the geometric

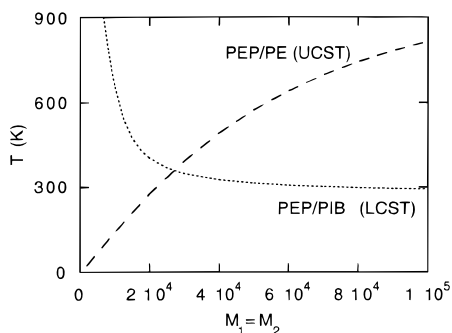


**Figure 8.** Molar mass dependence of the critical temperatures of PEP/PE and PEP/PIB blends at a pressure of 0.1 MPa as predicted with the aid of the simulation result  $g_{sim}$ , cf. Table 1 for the geometric correction.

mean prediction of 127 K. This corresponds to an underprediction of the miscibility of hhPP/PIB blends. For the PP/PIB blend, on the other hand, the simulations lead to an overprediction of the miscibility. This blend represents the only case, where the geometric mean,  $g = 1$ , yields a better prediction than  $g_{sim}$ . In summary, with respect to the PIB blends,  $g_{sim}$  is too small for the hhPP blend, just right for the PEP blend, and too large for the PP blend; this observation will be discussed in more detail below.

The remaining PEP blends in Table 1 exhibit UCST phase diagrams. At a mass fraction of 40% hhPP, experiments<sup>2</sup> find the PEP/hhPP blend to be phase separated at 324 K and in the one-phase region at 356 K. This behavior is reproduced by the BGY lattice model with  $g_{exp} - 1 = -0.75 \times 10^{-4}$ , while the simulations yield  $g_{sim} - 1 = -2.81 \times 10^{-4}$ , corresponding to a phase transition temperature of 773 K. For the PEP/PP blend, experimental data<sup>2,23</sup> on two blends were combined to establish boundaries on the correction factor with the result that  $-3.1 \times 10^{-4} < g_{exp} - 1 < -0.9 \times 10^{-4}$ . The simulation result  $g_{sim} = -0.917 \times 10^{-4}$  is just inside these boundaries. For the final blend of Table 1, PP/hhPP, both the geometric mean,  $g = 1$ , and the simulation result,  $g_{sim} - 1 = -3.72 \times 10^{-4}$ , reproduce the experimental observation of miscibility from 300–400 K.

It is interesting to shift the focus from individual blends and to compare properties of polyolefin blends with UCST phase diagrams to those with LCST phase diagrams. In Figure 8 we present predictions of the molar mass dependence of the critical temperatures for a UCST and an LCST blend. As expected, the miscibility decreases with increasing molar mass of the components for both types of blends. The values for the UCST, however, increase much more uniformly over the range of molar masses than the LCST values which decrease very rapidly for small molar masses but change very little for larger molar masses in agreement with experimental observation.<sup>3</sup> In Figure 9 we address the pressure dependence of UCSTs and LCSTs. As in the case of the pressure dependence of the spinodal temperatures of the hhPP/PIB blend, we set  $\bar{v} = (v_1 + v_2)/2$  in these calculations, where the values for  $v_1$  and  $v_2$  are given in Table 2. As before, the use of  $\bar{v}$  rather than  $v_0$  has little effect on the value of the LCST at atmospheric pressure changing it by 13 K. The value of the UCST, however, changes by about 110 K. The sensitivity of the transition temperatures to changes in  $v$  will be discussed further below. In qualitative agreement with experimental results for other polyolefin blends,<sup>5,24</sup> we

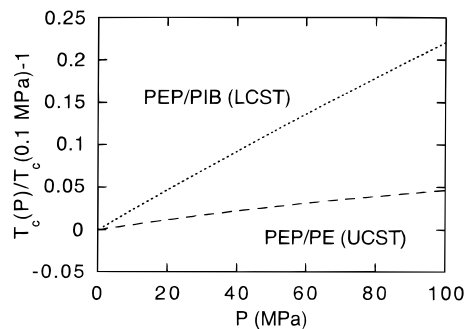


**Figure 9.** Relative pressure variation of the critical temperatures of the PEP/PE and PEP/PIB blends of Table 1 as predicted with the aid of the simulation result  $g_{sim}$  for the geometric correction.

find that increasing the pressure reduces the miscibility of the blend exhibiting a UCST and increases the miscibility of the LCST blend.

## 6. Discussion and Conclusions

In previous studies on small alkane mixtures we found that the geometric mean approximation for the mixed interaction energy yielded predictions which were in good to excellent agreement with experimental results for such quantities as the volume change on mixing and its pressure dependence, and the equilibrium vapor pressure above a solution as a function of concentration and temperature, this latter quantity being a direct measure of the free energy of the mixture. We also found that use of the geometric mean approximation resulted in predictions of the LCSTs of alkane–polyethylene solutions which were in close agreement with literature results for alkanes ranging from heptane through tridecane. Our predictions compared well with experiment not only for the critical point but also for the whole coexistence curve and its dependence on polymer molecular weight. Encouraged by this success, we began the research on polymer blends using the same approximation and found that agreement with experiment was not as good. In particular, the geometric mean approximation was unable to capture the effects leading to UCST behavior in these blends. The required corrections to  $\epsilon_{12}$ , although on the order of less than a tenth of a percent, are sufficient to change the miscibility predictions in a dramatic way. Thus, the relatively small difference in branching between the polyolefins is enough to differentiate the components such that limited miscibility may result, even though both components are saturated hydrocarbons. Indeed, the extent to which the geometric mean approximation applies may be used as a kind of indicator as to the similarity of the two components.

We next turned to the approach most widely found in the literature, viz. making use of experimental results to determine all of the required microscopic parameters. In our studies comparing the BGY predictions with experiment, we have used pure component data (*PVT* surfaces, liquid–vapor coexistence densities, etc.) in order to obtain the pure component parameters. Determination of  $\epsilon_{12}$  by the same kind of route requires the additional task of finding and using suitable data on the mixtures. The two kinds of data most commonly used for this purpose are critical point/coexistence results and small angle neutron scattering (SANS) data. We chose the former, although we are planning to make use of SANS data in the future. By using a single point

on a blend coexistence curve in order to determine the  $\epsilon_{12}$  value, we found that the quality of the predictions can change dramatically relative to those using the geometric mean approximation. For example, a factor of  $g_{\text{exp}} = 0.99956$  in eq 10 is required to obtain the experimental UCST of 421 K for PEP/PE, whereas the geometric mean value of  $g = 1$  results in a prediction of complete miscibility for this blend. Then, treating  $g_{\text{exp}}$  as a constant for a particular blend, we were able to make predictions for the effects of changing molecular weight on the coexistence curve in excellent agreement with experimental results. Similar results were obtained for the other blends where the geometric mean approximation fails. Our qualitative predictions regarding the sensitivity of UCSTs and LCSTs to changes in pressure are in agreement with experimental data. Whereas in the calculations at atmospheric pressure the value of the lattice volume was fixed to  $v_0 = 0.013$  L/mol for all components, for the high pressure studies we employed the arithmetic mean  $\bar{v} = (v_1 + v_2)/2$ , where  $v_i$  is the lattice volume of component  $i$ . The effect is to improve the predictions for the LCSTs at elevated pressures with little difference in their values at atmospheric pressure. The change in  $v$  has a greater impact on the UCSTs at all pressures. This is likely due to the fact that a decrease in  $v$  is correlated with an increase in  $r$ , needed to maintain a constant hard core volume  $rv$ . As a result, the number of nearest neighbor contacts increases. While an LCST may arise from equation of state effects or energetic asymmetries, the UCSTs considered in this work are always associated with the latter. Therefore an increase in the unfavorable contacts will lead to a higher value for the UCST, which is what we observe. Given these two approaches to the choice of  $v$ , it is sensible to use the average value  $\bar{v}$  for the blend of interest. In summary, we conclude that the BGY theory combined with suitable experimental results on the pure components and a modest set of data on the mixture is capable of making predictions about the effects on miscibility of changing all of the usual experimental variables (temperature, composition, pressure).

However, the main achievement of this work has been the development of a method whereby simple simulation methods (in fact, exact enumerations) are combined with the BGY theory in order to predict values for the factor  $g$ . This has allowed us to draw conclusions about the miscibility of the blends studied here without having to use any data on the mixtures themselves. As shown above, these predictions are in good to excellent agreement with the experimental results for all but the polypropylene blends with PEP and PIB, and even for most of these blends the predicted changes are in the right direction relative to the geometric mean results. The only exception is for the PP/PIB blend, where the predicted  $g$  value yields a blend of greater miscibility than the geometric mean would predict, the latter being in closer accord with experiment. Quantitatively, the predicted miscibility for both hhPP/PIB and PEP/hhPP is too small, whereas (as noted above) the predicted miscibility is too large for the PP/PIB blend, and is on the upper boundary for the PEP/PP blend. The simulation method presented in section 4 addresses packing effects in the interactions between straight sections of polymer chains. The fact that the simulation results do not reproduce the increased miscibility of hhPP over PP in either PEP or PIB blends suggests that more is at

work than the packing effects which can be accounted for using rigid-backbone sections of chain, as we have done here. One factor might be the imposition of rigidity to the backbone, presumably less of an issue for the more highly branched PIB than for PE. However, the BGY-simulation predictions for the PE/PEP blend are in close accord with experiment, unlike the geometric mean results. In addition, the predictions for the PE/PIB blend itself also compare favorably with experiment. Considering blends of PEP/hhPP and PEP/PP Freed and co-workers<sup>9</sup> also conclude that more is at play than packing effects alone, and point to differences in the bending energies of hhPP and PP chains. Alternatively, the different arrangements of the methyl groups along the hhPP and PP backbones and the resulting effects on the interaction energies along the chains may play an important role. Since the simulation method presented in section 4 can easily be adapted to include these effects, it will be possible to investigate causes for the differences in miscibility between PP and hhPP blends in the future.

The lattice BGY theory yields simple expressions for thermodynamic properties of equilibrium mixtures. One challenge facing all microscopic theories is working out a method of determining values for the parameters required for making theoretical predictions. Since it is widely accepted that use of pure fluid data is a reasonable route to the parameters characterizing the pure components this leaves determination of the mixed interaction energy as the problem. There is an additional challenge in applying the BGY theory to mixtures in which microscopic structure is believed to play an important role and that is how to account for the local structural detail. We have tackled both problems by making use of exact enumerations in order to predict the effect of branching on the mixed interaction energy. Comparison of our results with experimental data shows that this approach can account for some but not all of the influence of short branching on blend miscibility.

**Acknowledgment.** The authors would like to thank D. J. Lohse for supplying *PVT* data for the polymers, and M. Rabeony for providing data on hhPP/PIB blends prior to publication. Financial support from the National Science Foundation (Grant DMR-9730976) and the Camille and Henry Dreyfus Foundation is gratefully acknowledged.

#### Appendix: Determination of BGY Parameters for the Polyolefins

For one-component fluids, eqs 1–4 of the BGY lattice model are evaluated with  $K = 1$  so that we drop the subscripts. The system-dependent parameters are then the number  $r$  of segments per molecule, the volume  $v$  per lattice site, and the interaction energy  $\epsilon$ . For each of the polyolefins of interest these parameters were determined from a comparison of eq 4 with experimental pressure-volume-temperature (*PVT*) data.<sup>25</sup> For sufficiently long polymer chains, the *PVT* surface expressed in terms of specific volume or mass density is independent of the molar mass.<sup>4,26</sup> The BGY lattice model, on the other hand, employs number densities and thus a value for the molar mass  $M$  is required in the interpretation of experimental data. In accordance with the observation above, the particular value of  $M$  does not affect the quality of the description of the experimental

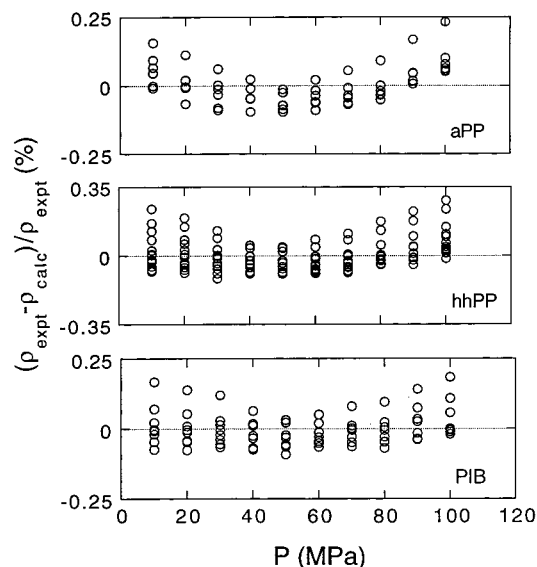


**Figure 10.** Percent deviations between experimental<sup>25</sup> and calculated (eq 4) with system-dependent parameters  $r$ ,  $v$ , and  $\epsilon$  from Table 2) values of the densities of three of the polyolefins considered in this work.

*PVT* data as long as  $M$  is sufficiently large. In this case, of the three parameters,  $r$ ,  $v$ , and  $\epsilon$ , only the number  $r$  of segments per molecule is affected by the choice of  $M$  and is indeed proportional to it.<sup>17</sup> We are therefore free to fix the value of  $M$  to  $M_0 = 170\,000$  in the determination of the system-dependent parameters and later rescale the value of  $r$ , cf. eq 15, to match the desired molar mass. Experimental<sup>25</sup> and calculated *PVT* data in a pressure range from 10 to 100 MPa and a temperature range from 400 to 500 K were compared to determine the BGY parameters for high density polyethylene (hdPE), PEP, atactic polypropylene (aPP), hhPP, and PIB. For hdPE and aPP, furthermore, data with temperatures below 423.8 and 435.4 K, respectively, were excluded so as to stay comfortably above the melting transition.<sup>26</sup> Except for the boundaries of the temperature–pressure range, the BGY lattice model yields an excellent representation of the *PVT* data. The reduced  $\chi^2$  values for the fits based on an experimental error in the specific volume of 0.001 mL/g<sup>26</sup> range from  $\chi^2 = 0.45$  for PIB to  $\chi^2 = 1.2$  for PEP. In Table 2, we present the system-dependent parameters, and in Figure 10 are presented the relative density deviations between experimental and calculated densities for the polyolefins considered in this work.

When the BGY lattice model is applied to binary mixtures, it is most convenient to employ a common value  $v_0$  for the volume per lattice site. Given that the representation of the *PVT* surface depends more strongly on the hard-core volume  $rv$  of the molecules, than on either  $r$  or  $v$  alone, it is natural to choose a value  $v_0$  for the volume per site and then rescale the segment number according to  $r \rightarrow (rv)/v_0$ . Since most of the available miscibility data were obtained at atmospheric pressure, it is important that the value for  $v_0$  together with the value of  $(rv)/v_0$  yield a good description of the *PVT* surface at low pressures. In this work we adopt  $v_0 = 0.013$  L/mol and show in Figure 11 a comparison of experimental densities of hdPE with those calculated with the aid of the original ( $r$ ,  $v$ ) and rescaled ( $(rv)/v_0$ ,  $v_0$ ) parameters, respectively. While the rescaled parameters lead to large deviations for the higher pressures the deviations become smaller with decreasing pressure

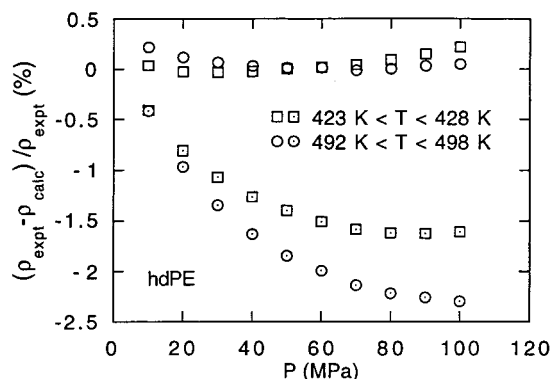


**Figure 11.** Effect of rescaling the system dependent parameters. Shown are the percent deviations between experimental<sup>25</sup> and calculated values of the densities of polyethylene for the highest and lowest temperatures considered. The open symbols were obtained with the aid of eq 4 and the fit parameters ( $r$ ,  $v$ ) from Table 2; the dotted symbols correspond to the rescaled parameters ( $(rv)/v_0$ ,  $v_0$ ).

and may even yield a better description of the *PVT* surface at atmospheric pressure than the original parameters.

Finally, in contrast to *PVT* properties, phase separation is strongly affected by the molar mass of the polymers so that we need to be able to describe polymer blends with constituents of various molar masses. Since the segment number is proportional to the molar mass<sup>17</sup> the value  $r(M)$  for a given molar mass  $M$  is obtained by

$$r(M) = M \frac{(rv)}{v_0 M_0} \quad (15)$$

where the values of  $(rv)/(v_0 M_0)$  are quoted in Table 2.

## References and Notes

- Bates, F. S.; Schulz, M. F.; Rosedale, J. H. *Macromolecules* **1992**, *25*, 5547.
- Graessley, W. W.; Krishnamoorti, R.; Reichart, G. C.; Balsara, N. P.; Fetters, L. J.; Lohse, D. J. *Macromolecules* **1995**, *28*, 1260.
- Krishnamoorti, R.; Graessley, W. W.; Fetters, L. J.; Garner, R. T.; Lohse, D. J. *Macromolecules* **1995**, *28*, 1252.
- Krishnamoorti, R.; Graessley, W. W.; Dee, G. T.; Walsh, D. J.; Fetters, L. J.; Lohse, D. J. *Macromolecules* **1996**, *29*, 367.
- Rabeony, M.; Lohse, D. J.; Garner, R. T.; Han, S. J.; Graessley, W. W.; Migler, K. B. Preprint.
- Dudowicz, J.; Freed, K. F. *Macromolecules* **1996**, *29*, 8960.
- Foreman, K. W.; Freed, K. F. *Macromolecules* **1997**, *30*, 7279.
- Foreman, K. W.; Freed, K. F.; Ngola, I. M. *J. Chem. Phys.* **1997**, *107*, 4688.
- Freed, K. F.; Dudowicz, J.; Foreman, K. W. *J. Chem. Phys.* **1998**, *108*, 7881.
- Rajasekaran, J. J.; Curro, J. G.; Honeycutt, J. D. *Macromolecules* **1995**, *28*, 6843.
- Melenkevitz, J.; Curro, J. G. *J. Chem. Phys.* **1997**, *106*, 1216.
- Singh, C.; Schweizer, K. S. *Macromolecules* **1997**, *30*, 1490.
- Luettmmer-Strathmann, J.; Schoenhard, J. A.; Lipson, J. E. G. *Macromolecules*, in press.
- Taylor, J. K.; Debenedetti, G.; Graessley, W. W.; Kumar, S. K. *Macromolecules* **1996**, *29*, 764.
- Lipson, J. E. G.; Andrews, S. S. *J. Chem. Phys.* **1992**, *96*, 1426.
- Lipson, J. E. G.; Brazhnik, P. K. *J. Chem. Phys.* **1993**, *98*, 8178.
- Luettmmer-Strathmann, J.; Lipson, J. E. G. *Fluid Phase Equilib.* **1998**, *150–151*, 649.
- Lipson, J. E. G. *Macromol. Theory Simul.* **1998**, *7*, 263.
- Tompa, H. *Polymer Solutions*; Butterworths: London, 1956.
- Sanchez, I. C.; Lacombe, R. H. *Macromolecules* **1978**, *11*, 1145.
- Rowlinson, J. S.; Swinton, F. L. *Liquids and liquid mixtures*, 3rd ed.; Butterworths: London, 1982.

- (22) Unpublished values for spinodal temperatures of hhPP/PIB blends were made available to us by M. Rabeony.
- (23) Lohse, D. J.; Fetters, J. L.; Doyle, M. J.; Wang, H.-C.; Kow, C. *Macromolecules* **1993**, *26*, 3444.
- (24) Hammouda, B.; Balsara, N. P.; Lefebvre, A. A. *Macromolecules* **1997**, *30*, 5572.
- (25) Tabulated values for the *PVT* properties of the polyolefins were made available to us by D. J. Lohse.
- (26) Walsh, D. J.; Graessley, W. W.; Datta, S.; Lohse, D. J.; Fetters, J. L. *Macromolecules* **1992**, *25*, 5236.

MA981478E